ACS Catalysis

Research Article

pubs.acs.org/acscatalysis

Methanol to Dimethyl Ether over ZSM-22: A Periodic Density Functional Theory Study

Poul Georg Moses*,† and Jens K. Nørskov

SUNCAT Center for Interface Science and Catalysis, Department of Chemical Engineering, Stanford University, Stanford, California 94305, United States and SLAC National Accelerator Laboratory, 2575 Sand Hill Road, Menlo Park, California 94025, United States

Supporting Information

ABSTRACT: Methanol-to-DME conversion over ZSM-22 Brønsted acid sites is investigated on the basis of periodic density functional theory calculations. DME formation has been speculated to take place via the dissociative or associative pathway. It is shown that the dissociative pathway is the predominant pathway. We find that water lowers the activation energies of key reactions but that the lowering of the activation energies is insufficient to increase the rate because of the entropy loss associated with water adsorption. The consequence of acid strength on the methanol-to-DME conversion pathways is investigated on the basis of Al-, Ga-, or In-induced Brønsted acid sites. We show that linear correlations between activation energies and acid strength exist. It is found that weaker acidity leads to higher activation energies. We find that changes in acidity will not change the conclusion that the dissociative pathway is the predominant pathway.

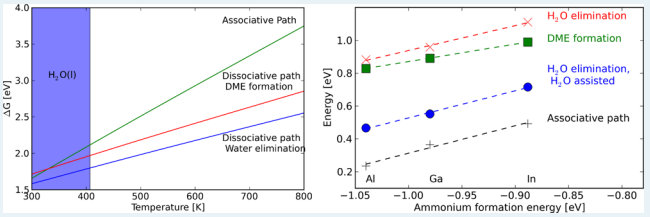

KEYWORDS: *DME,DFT, ZSM-22, acidity, zeolites, kinetics*

1. INTRODUCTION

Dimethyl ether (DME) has attracted widespread attention because of its possible use as a substitute for liquefied petroleum gas (LPG) for household applications or diesel fuel for transportation.[1−3] Better understanding of the reaction networks involved in DME synthesis and their relative importance under reaction conditions is needed to improve properties such as temperature tolerance, selectivity, and tendency toward coke formation.[4,5] The DME reaction network has been proposed to include two different pathways, termed the associative pathway and the dissociative pathway (see Figure 1).[6−9] Both pathways are believed to take place at Brønsted acid sites.[8,10−15] The associative pathway, which is also known as the direct or concerted pathway, is defined by coadsorption of two methanol molecules, which react and form DME directly. The dissociative pathway, which is also known as the stepwise or consecutive pathway, is defined by initial methanol adsorption, followed by water elimination from methanol, leading to adsorbed methyl and water. The methyl group acts as a methylating agent and reacts with a second methanol to form DME, but the role and importance of methyl groups in DME synthesis are not fully understood.[8,15,16] The existence of methyl groups cannot be taken as direct evidence of the dissociative pathway being faster than the associative pathway. The acidity of the DME catalyst influences the catalytic properties,[4,5] but no clear picture exists on how acidity influences the different DME reaction pathways.

Density functional theory (DFT) has been used in several studies to investigate DME synthesis. The DFT studies have used two different models, one based on clusters and one on periodic systems, with the cluster model as the most common approach. Zeolites are periodic structures, and it has been shown that convergence of cluster models to the periodic representation requires large clusters.[17] Therefore, periodic models should, in principle, be preferred over cluster models.[17] However, because of the large size of most zeolite unit cells, computational resources have limited the number of periodic studies. Small cluster models, on the other hand, present a much faster alternative, and the two most comprehensive studies on DME synthesis over zeolites have been based on cluster models.[6,13]

The earliest study used a 3 T sites cluster, that is, the periodic zeolite structure was represented by 2 Si atoms and one Al atom and surrounding O atoms.[6] The main conclusion drawn on the basis of the 3T cluster model was that the associative pathway will dominate, as a result of significantly higher barriers for the dissociative pathway.[6] This conclusion was later strengthened by a study using a slightly larger cluster model with 5T sites.[13] The sizes of clusters in both studies are quite small, in the first case, probably dictated by the available computer resources at the time, and in the second study, the focus was broader than DME synthesis, and a less accurate cluster was justified by the large number of reaction steps involved in the study. Cluster sizes of 3 or 5 T sites are both very far from being converged,[17] and one could speculate that periodic models would give significantly different results.

Periodic studies for DME synthesis have unfortunately been limited to narrow 8 ring pore zeolites and calculations of

Received: November 9, 2012
Revised: January 29, 2013
Published: February 26, 2013

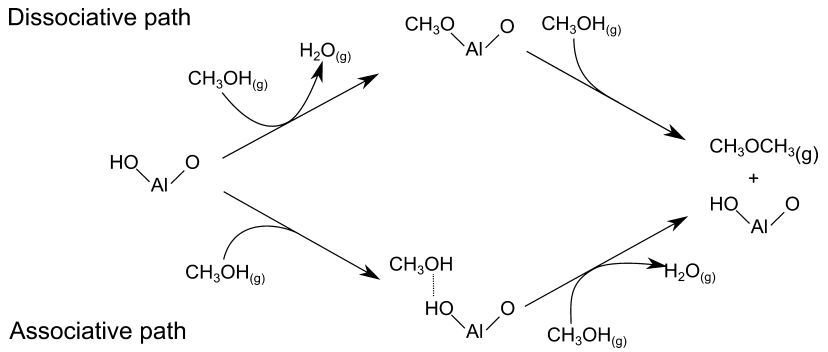

Figure 1. The dissociative and the associative pathways for the methanol-to-dimethyl ether reaction.

energies of reaction intermediates,[11] whereas calculations of activation energies have been limited to the activation energy of the associative pathway[12,18] and not extended to the full reaction network. Periodic DFT calculations on 8 ring zeolites[11,12,18−20] have been used to elucidate experimental studies, suggesting that protonated methanol plays an important role in DME synthesis[8] and showing that a high coverage of methanol or geometric constraints may lead to stabilization of protonated methanol.[21] Direct comparison of cluster and periodic studies for the methylation of toluene has shown that cluster models have a tendency to overestimate barrier heights,[22] which is also what is seen for the barriers of the associative pathway in DME synthesis,[12,18] even though the differences in barriers could also be attributed to different approximations within the specific implementations of DFT.

In addition to studies on DME synthesis over zeolites, DFT has also been used to investigate DME synthesis over tungsten polyoxometalate Kegging clusters.[10] In this recent study, it was concluded that the associative pathway dominates on tungsten polyoxometalate Kegging clusters.[10] Furthermore, a correlation between acidity of the Kegging clusters and barrier heights was identified. Thus, insight into the effect of changing acidity for tungsten polyoxometalate Kegging clusters[10] was gained, which could potentially lead to rational design of catalysts. However, tungsten polyoxometalates are stronger acids than zeolites, and it is not clear whether the correlations found can be extrapolated to the range of acidities available in zeolites.

The present study investigates the associative and dissociative pathway in a periodic system. We focus on ZSM-22, which has a 1D channel system with 10 ring pores. ZSM-22 has attracted interest because of its unique topology, which suppresses formation of aromatics and changes the selectivity in methanol to hydrocarbon[23−30] reactions. One of the challenges in DME synthesis is to avoid coke formation, and since aromatics and hydrocarbons are possible precursors to coke, it may therefore be speculated that ZSM-22, when used as a DME synthesis catalyst, could have a higher resistance against coke formation than other zeolites. Coke formation is outside the scope of the present study, but a detailed understanding of DME synthesis and the influence of acidity on activity is an important prerequisite to understanding coke formation.

We investigate DME synthesis over single Brønsted acid sites. We include the possible effects of coadsorbed water because studies on cluster models have shown that coadsorption of water may change the activation energies of key reaction steps.[13,31] We also investigate the influence of changes in acidity on activity. Zeolite acidity is a function of the zeolite structure and the nature of the substitutional cations. The most common substitutional cation is Al, but Ga and In substitution may also be used to tune the acidity.[32] We use the ammonium ion formation energy as a measure of acidity and vary the acidity by doping with Al, Ga, or In and thereby present, to the best of our knowledge, the first DFT study on the effect of cation substitution in zeolites on acidity.

We find that the dissociative pathway dominates over the associative pathway at industrially relevant conditions and that water has no beneficial effect on the rate of DME synthesis. We find that weaker acidity leads to higher activation energies. Activation energies are found to depend linearly on the acidity. We also find that the activation energies in the dissociative and the associative pathways have very similar linear correlations with acidity. This indicates that the relative importance of the dissociative pathway with respect to the associative pathway is not influenced by changes in acidity.

2. CALCULATIONAL DETAILS

The density functional theory calculations are carried out with the DFT code GPAW with the ASE interface.[33] GPAW is based on the projector-augmented wave (PAW) method. GPAW uses real-space uniform grids and multigrid methods.[34,35] We use the RPBE exchange correlation functional[36] and a real-space grid spacing of 0.18 Å. The ZSM-22 zeolite is represented by the primitive unit cell repeated twice along the channel directions (see Figure 2), and we use a k-point sampling of 2 × 2 × 2 k-points for the repeated primitive unit cell. The optimized lattice constants for the conventional cell are found to be [14.33, 18.15, 5.33 Å], which are slightly larger than experimental values [13.859, 17.420, 5.038 Å].[37] The convergence criterion for structural optimization is a maximum force of 0.03 eV/Å per atom, that is, the force on each

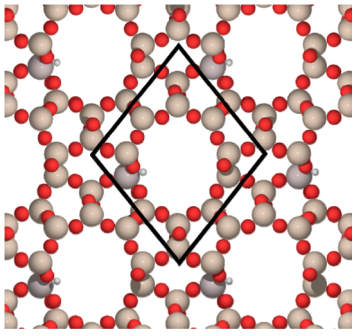

Figure 2. ZSM-22 crystal structure. The black line marks the primitive unit cell. Color code: Si, sand; Al, gray; H, white.

dx.doi.org/10.1021/cs300722w | ACS Catal. 2013, 3, 735−745

individual atoms is lower than 0.03 eV/Å. Transition states are located using the nudged elastic band algorithm with the climbing image method.[38]

Gibbs free energies are calculated using

$$G(T) = E_{\mathrm{DFT}} + E_{\mathrm{vib}}^{0\,\mathrm{K}} + \mathrm{d}H_{0-298.15\mathrm{K}} + \mathrm{d}H_{298.15-T} - TS^{T} \quad \text{(Eq 1)}$$

:where E_{DFT} is the electronic energy, $E_{\mathrm{vib}}^{0\,\mathrm{K}}$ is the vibrational zero point energy, $\mathrm{d}H_{0-298.15\ \mathrm{K}}$ is the enthalpy change from 0 K to 298.15 K, $\mathrm{d}H_{298.15-T}$ is the enthalpy change from 298.15 K to the temperature T, and S^T is the entropy at temperature T. For surface structures, all terms in $G(T)$, including $\mathrm{d}H_{0-298.15\ \mathrm{K}}$ and $\mathrm{d}H_{298.15-T}$ are calculated in the harmonic approximation on the basis of the calculated vibrational frequencies. For gas phase molecules, the entropy and both enthalpy terms ($\mathrm{d}H_{0-298.15\ K}$ and $\mathrm{d}H_{298.15-T}$) in $G(T)$ are calculated using data from refs 39 and 40.

We base the first principles thermodynamics on vibration frequencies calculated in the harmonic approximation. The harmonic approximation has previously been shown to give accurate results for many different heterogeneous catalytic reactions.[41] However, the harmonic approximation has also been shown to underestimate the entropy of adsorbed species and transition states in propane cracking over acid zeolites.[42,43] It could be speculated that the effect is smaller for DME synthesis because the reactants are more strongly bound than propane at the acid site. Nevertheless, it could be interesting in future studies to go beyond the harmonic approximation.

3. RESULTS AND DISCUSSION

The associative and dissociate pathways are investigated, including the possible effects of coadsorbed water. The two pathways are investigated on the same active site located as seen in Figure 2. The active site is a Brønsted acid site. Brønsted acid sites are created by substitution of Si atoms with atoms that act as electron acceptors. The most commonly used acceptor is Al. The charge neutrality of the zeolite crystal is maintained by protons attached to O atoms attached to the Al dopant. Al may substitute several different sites, and we investigate the Brønsted acid site with the lowest electronic energy.

We investigate the influence of intrinsic acidity on the active site activity by varying the Brønsted acidity of ZSM-22 by substituting Al with Ga or In, thus investigating how activity correlates with changes in acidity due to electronic effects and not geometric effects.

3.1. The Associative Pathway. The potential energy diagram for the associative pathway is seen in Figure 3, the structure of the transition state is seen in Table 1, and the structures of the intermediates are seen in Table S1 in the Supporting Information. The associative pathway is initiated by adsorption of one CH_3OH (ΔE = −0.63 eV). The adsorbed CH_3OH forms a hydrogen bond with the acid site, with O in the hydroxyl group pointing toward the acid proton and H in the hydroxyl group pointing toward one of the O atoms neighboring the Al atom. Adsorption of the first CH_3OH molecule is followed by adsorption of a second CH_3OH molecule (ΔE = −0.4 eV). The two CH_3OH molecules form a hydrogen bond network with the acid site where the proton becomes solvated. Our results indicate that solvation of the proton is spontaneous because among all the configurations investigated, the proton moves from the acid site to the methanol dimer to form a protonated methanol dimer. This

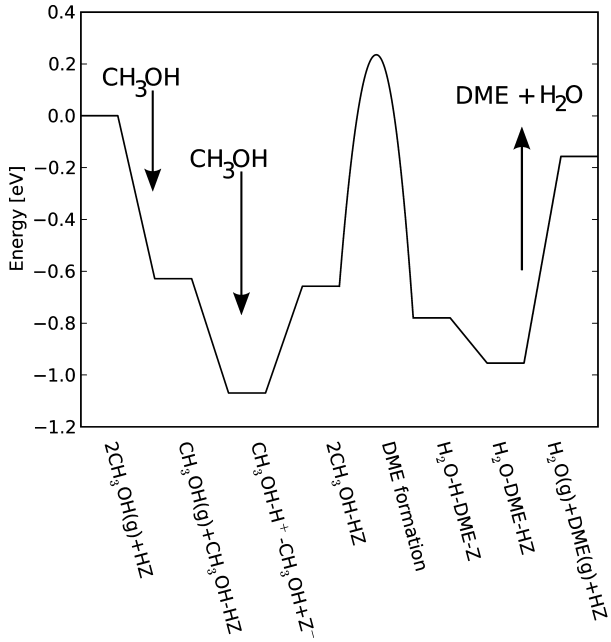

Figure 3. Electronic energies for intermediates and transition states along the associative pathway.

finding is in agreement with earlier studies on 8 ring pores;[21] however, the protonated-methanol-dimer-acid-site complex has to be broken to reach the initial state of the DME formation reaction (ΔE = 0.41 eV, see Figure 3). The complex is broken because in the initial state, the methyl group of one methanol points toward the hydroxyl group of the other methanol; thus, the proton is now bound to the acid site, and methanol is not protonated. From the initial state, the two methanols and the proton react and form water and DME (energy barrier of 0.89 eV relative to the initial state and 0.2 eV relative to the gas phase reference). In the transition state, the carbon and hydrogens belonging to the methyl group of one of the CH_3OH's are in the same plane, and the O−C−O atoms form an almost straight line, with a bond angle of 178° (see Table 1). The methyl group thereby undergoes an umbrella flip and forms DME and water. The product state then reorganizes and forms a slightly more stable adsorbed DME and water (ΔE = −0.17 eV). Finally, DME and water desorb and leave behind a proton, regenerating the active site (ΔE = 0.80 eV).

As mentioned above, DFT studies on cluster models have shown that coadsorption of water changes the activation energies of key reaction steps.[13,31] We have therefore investigated the effect of coadsorption of water on the associative pathway as seen in Figure 4. The structure of the intermediates can be seen in the Supporting Information in Table S2. Adsorption of water stabilizes methanol by −0.32 eV (see Figure 4). Water forms a hydrogen bond with methanol and forms a protonated methanol−water complex. Adsorption of a second methanol molecule forms a proton methanol dimer which is stabilized by −0.38 eV by the coadsorbed water. Coadsorption of water allows the formation of DME and water directly without breaking the hydrogen bond network and leads to lowering of the activation energy by 0.24 eV, compared with the water-free reaction. The transition state geometry is similar to the transition state without water. The C and H belonging to methanol's methyl group are in the same plane, and the O−C−O atoms form an almost straight line with a bond angle of 173° (see Table 1). The coadsorbed water binds to the water being

dx.doi.org/10.1021/cs300722w | ACS Catal. 2013, 3, 735−745

Table 1. Structures of Transition States in the Associative and Dissociative Pathway with and without Water

Reaction	Product geometry	Distances				angle	ΔEref	Ea
	Front	0-1	1-2	2-3	3-4			
		[Å]	[Å]	[Å]	[Å]	Deg.	[eV]	[eV]
$CH_3OH_2Z \rightarrow H_2O\text{-}CH_3\text{-}Z$	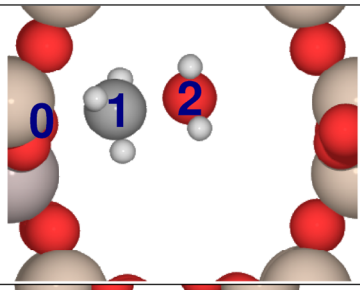	2.17	1.95			177	0.88	0.69
$H_2O\text{-}H\text{-}CH_3OH\text{-}Z \rightarrow 2H_2O\text{-}CH_3\text{-}Z$	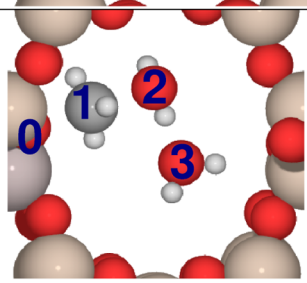	2.01	2.05	2.71		176	0.47	1.41
$CH_3OH\text{-}CH_3\text{-}Z \rightarrow DME\text{-}HZ$	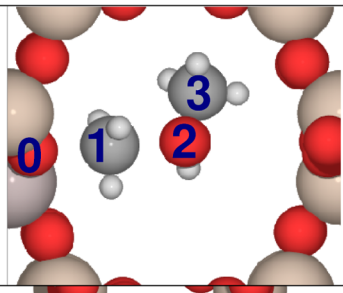	2.04	2.00	1.47		177	0.83	0.86
$CH_3OH\text{-}H\text{-}CH_3OH\text{-}Z \rightarrow H_2O\text{-}H\text{-}DME\text{-}Z$	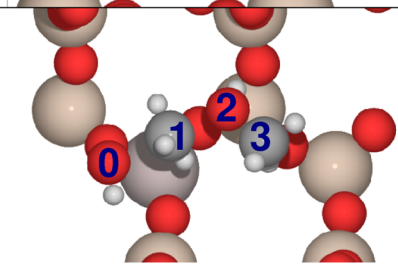	2.04	1.97	1.47		178	0.23	0.89
$H_2O\text{-}CH_3OH\text{-}H\text{-}CH_3OH\text{-}Z \rightarrow H_2O\text{-}H\text{-}DME\text{-}H_2O\text{-}Z$	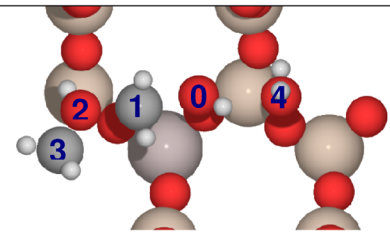	2.05	1.93	1.47	2.88	173	-0.01	1.00

eliminated from methanol and thereby lowers the energy of the transition state relative to the case in which no water is coadsorbed (see Table 1).

3.2. The Dissociative Pathway. In Figure 5, the potential energy diagram for the dissociative pathway is seen, and the corresponding structures of the transitions states are seen in Table 1. The structures of the intermediates are seen in Table S3 in the Supporting Information. The dissociative pathway is initiated by methanol adsorption (ΔE = −0.63 eV). The adsorbed methanol reacts with the proton from the acid site and rotates to form a protonated methanol. The barrier for rotation is almost identical (0.84 eV) to the energy change (0.82 eV), and the barrier is therefore of no importance for the kinetics and has been left out of Figure 5 to reduce the complexity of the figure. Water is then eliminated from the protonated methanol, and a surface methyl is formed. The energy barrier for water elimination is 0.69 eV relative to the initial state and 0.88 eV relative to the acid site and gas phase

dx.doi.org/10.1021/cs300722w | ACS Catal. 2013, 3, 735−745

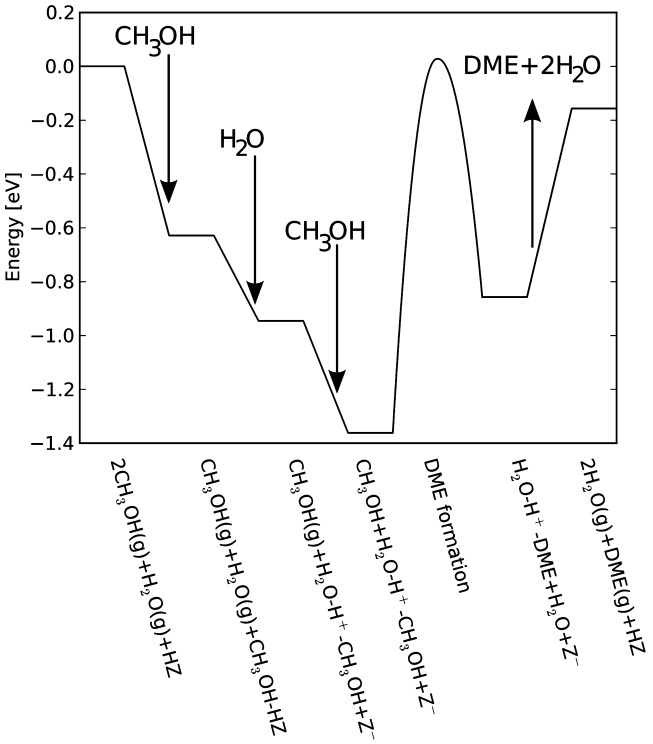

Figure 4. Electronic energies for intermediates and transition states along the associative pathway assisted by water.

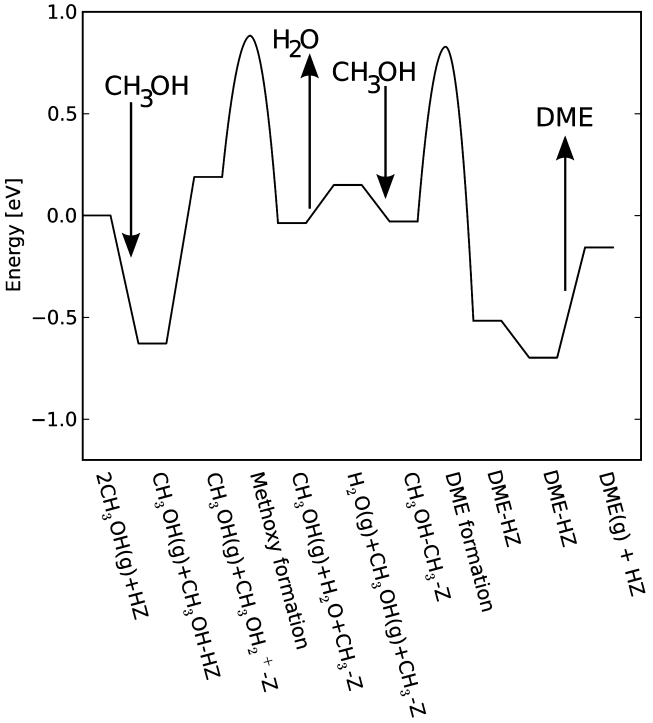

Figure 5. Electronic energies of intermediates and transition states along the dissociative pathway.

reactant. The geometry of the transition state is characterized by H and C atoms from the methanol methyl group being located in the same plane and an O−C−O bond angle of 177°, which is again very close to a straight line (see Table 1). The water elimination step is followed by water desorption (ΔE = 0.19 eV) and subsequently methanol adsorption (ΔE = −0.18 eV). The adsorbed methanol and the surface methyl then react and form DME with an activation energy relative to the initial state of 0.86 eV and 0.83 eV relative to the reference state (the acid site and gas phase reactants). Note that the transition state energies relative to the gas phase reactants and the acid site for the water elimination and DME formation reactions are almost equal, with an energy change of 0.88 eV for the water elimination step and 0.83 eV for the second step leading to DME.

We have also investigated a reaction pathway in which the water elimination step is assisted by coadsorption of water (see Figure 6 for the potential energy diagram and Table 1 for the

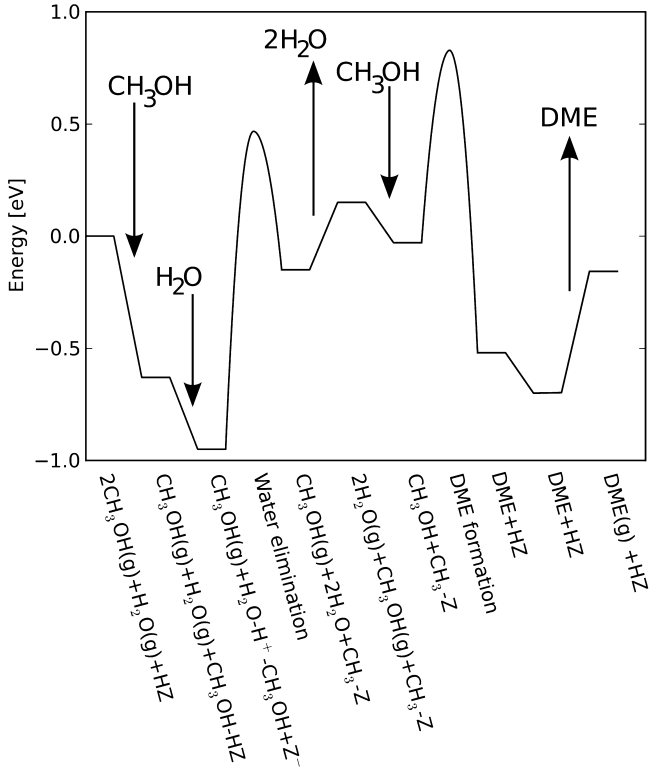

Figure 6. Electronic energies for intermediates and transition states along the dissociative pathway assisted by water.

structures and reaction energies of the transition states.; the structures of the intermediates can be seen in Table S4 in the Supporting Information). The water−methanol dimer is identical to the water−methanol dimer described for the associative pathway; however, in the context of the dissociative pathway, the coadsorption of water stabilizes the protonated methanol, and in contrast with the non-water-assisted reaction path, no intermediate protonated methanol state is found. Instead, the entire water−proton−methanol complex rotates and forms water and a surface methyl group. The structure of the transition state is similar to the structure with no water adsorbed, with an almost linear O−C−O angle of 176° and the C and H atoms from the methanol methyl group in the same plane. The coadsorped water is coordinated to the water being eliminated from methanol (see Table 1). The energy barrier relative to the initial state is 1.41 and 0.47 eV relative to the gas phase reactants and the acid site. Thus, we find that coadsorption of water leads to a 0.42 eV lowering of the energy relative to the gas phase reactants and the acid site.

dx.doi.org/10.1021/cs300722w | ACS Catal. 2013, 3, 735−745

3.3. Relative Importance of the Dissociative and Associative Pathways. In the following, we discuss the relative importance of the associative and dissociative pathways as a function of temperature and coadsorption of water. The associative pathway involves two methanol molecules, whereas the two steps in the dissociative pathway involve only one methanol molecule each. This could for entropy reasons lead to different temperature dependence of the two pathways and might lead to a crossover temperature above which the dissociative pathways would dominate.

To quantify the discussion of the relative rates, we have derived rate expressions for the two pathways by assuming that the rate of the associative pathway is determined by the DME formation step and the rate of the dissociative pathway is determined by the slowest of the water elimination step or the DME formation step. The rate expression of DME formation by the dissociative pathway is derived in two different cases: (i) the case in which the water elimination step is limiting and (ii) the case in which the DME formation step is limiting. These two rates can then be compared, and the rate of the dissociative path will then be the slower of the two cases.

In the following, we derive the rate expressions as given by the quasiequilibrium approximation, the irreversible step approximation, and in the limit of low methanol coverage. On the basis of previous studies on ammonia synthesis,[44] we assume that tunneling effects do not influence rates for DME synthesis at relevant industrial conditions. In addition, it is assumed that there is no mass-transfer limitation and that the activities of products and reactants in the zeolite are equal to the activities of gases in the bulk of the gas phase. Furthermore, we assume that the acid sites do not interact with each other and that they do not interact with molecules adsorbed on non-acid sites in the zeolite. This corresponds to assuming that the coverage of molecules on non-acid sites is small. In the limit of high coverage on acid as well as non-acidic sites, care should be taken when deriving rate equations using a mean field approximation.[42,43] Following the derivation of the rate expressions, we test our assumptions and show that under typical DME reaction conditions, all of the above approximations are valid and that the relative importance of the dissociative and associative pathway may be understood on the basis of the differences in Gibbs free energies between the transition state of the dissociative and associative pathway.

The rate expression for the DME formation step in the dissociative pathway is based on the following three reactions: $CH_3OH(g) + HZ \overset{K_{methyl}}{\longleftrightarrow} H_2O(g) + CH_3Z$, $CH_3OH(g) + CH_3Z \underset{\overleftarrow{k}_{diss,DME}}{\overset{\vec{k}_{diss,DME}}{\longleftrightarrow}} DME{-}HZ$, and $DME{-}HZ \overset{K_{DME}}{\longleftrightarrow} DME(g) + HZ$, where K_{methyl} and K_{DME} are the corresponding equilibrium constants and $\vec{k}_{diss,DME}$ and $\overleftarrow{k}_{diss,DME}$ are the forward and reverse rate constants, respectively. In the quasiequilibrium approximation, it is assumed that one step determines the rate and that all other steps are sufficiently fast that they can be considered as being in quasiequilibrium. In this approximation, the rate of the DME formation step in the dissociative pathway is given by eq 2.

$$r_{diss,DME} = \left(\frac{P_{CH_3OH}^{\ 2}}{P_{H_2O}} \vec{k}_{diss,DME} K_{methyl} - P_{DME} \frac{\overleftarrow{k}_{diss,DME}}{K_{DME}} \right) \theta_H,$$

$$\theta_H = \frac{1}{\frac{P_{DME}}{K_{DME}} + K_{methyl} \frac{P_{CH_3OH}}{P_{H_2O}} + 1} \tag{2}$$

In the irreversible step approximation, the quasiequilibrium approximation is further simplified by assuming that the reverse rate is much slower than the forward rate (see eq 3).

$$r_{diss,DME,irreversible} = \vec{k}_{diss,DME} K_{methyl} \frac{P_{CH_3OH}^{\ 2}}{P_{H_2O}} = \frac{P_{CH_3OH}^{\ 2}}{P_{H_2O}} \frac{k_B T}{h} \exp(-\Delta G^{TS}_{diss,DME}/k_B T) \tag{3}$$

Where, $\Delta G^{TS}_{diss,DME}$ is the change in free energy from the gas phase molecules to the transition state, k_B is the Boltzmann's constant, and h is the Planck's constant.

The rate expression for the water elimination step in the dissociative pathway ($r_{diss,water}$) is based on the following two reactions: $CH_3OH(g) + HZ \overset{K_{CH_3OH}}{\longleftrightarrow} CH_3OH{-}HZ$ and $CH_3OH{-}HZ \overset{\vec{k}_{diss,water}}{\longrightarrow} CH_3Z + H_2O(g)$. In the irreversible step approximation the rate of the water elimination step is given by eq 4

$$r_{diss,water} = \vec{k}_{diss,water} \frac{K_{CH_3OH} P_{CH_3OH}}{1 + K_{CH_3OH} P_{CH_3OH}} \tag{4}$$

which in the low coverage approximation simplifies to eq 5.

$$r_{diss,water,low} = \vec{k}_{diss,water} K_{CH_3OH} P_{CH_3OH} = P_{CH_3OH} \frac{k_B T}{h} \exp(-\Delta G^{TS}_{diss,water}/k_B T) \tag{5}$$

The rate expression for the associative pathway ($r_{associative}$) is based on the following two reactions: $CH_3OH(g) + HZ \overset{K_{CH_3OH}}{\longleftrightarrow} CH_3OH{-}HZ$ and $CH_3OH(g) + CH_3OH{-}HZ \overset{\vec{k}_{asso}}{\longrightarrow} DME(g) + H_2O(g) + HZ$. In the irreversible step approximation, the rate of the associative pathway is given by eq 6.

$$r_{associative} = \vec{k}_{asso} \left(\frac{K_{CH_3OH} P_{CH_3OH}}{1 + K_{CH_3OH} P_{CH_3OH}} \right) P_{CH_3OH} \tag{6}$$

In eq 6, we have furthermore assumed that the coverage of the second methanol is low, which is justified by the weaker adsorption by the second methanol than by the monomer methanol (−0.44 eV compared with −0.63 eV)

Equation 6 simplifies to eq 7 in the low-coverage approximation.

$$r_{associative,low} = \vec{k}_{asso} K_{CH_3OH} P_{CH_3OH}^{\ 2} = P_{CH_3OH}^{\ 2} \frac{k_B T}{h} \exp(-\Delta G^{TS}_{associative}/k_B T) \tag{7}$$

To study the relative rates of the two pathways, we use the following conditions: P_{CH_3OH} = 16 bar, P_{H_2O} = 3 bar, and P_{DME} = 1 bar, which represents typical DME synthesis conditions.[5] In the following analysis, we use the irreversible step approx-

dx.doi.org/10.1021/cs300722w | ACS Catal. 2013, 3, 735−745

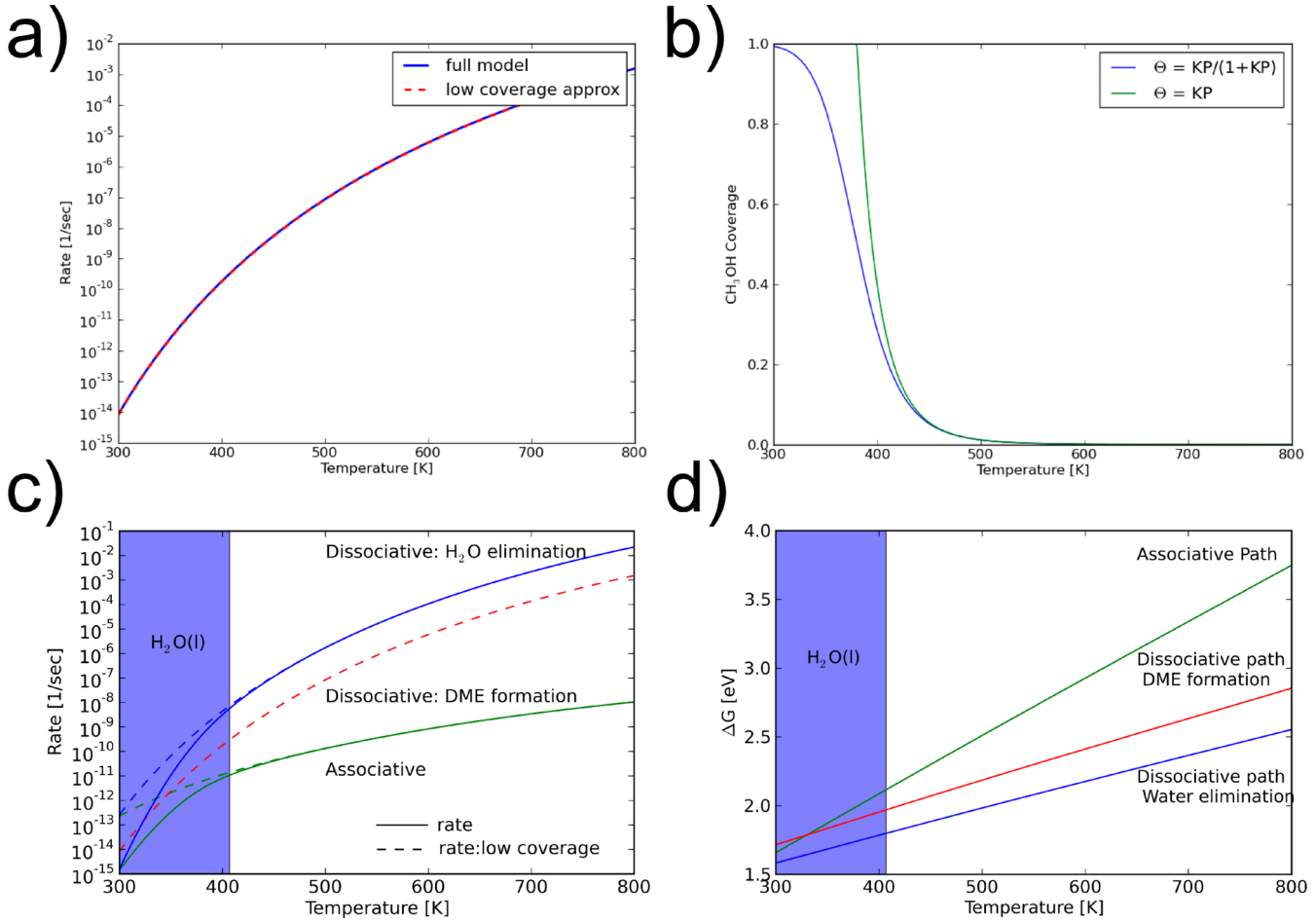

Figure 7. (a) The rate of the DME formation step in the dissociative path, calculated within the quasiequilibrium approximation or the irreversible step approximation. (b) The coverage of methanol as a function of temperature. (c) The rate of the three different reactions in DME synthesis, calculated within the irreversible step approximation. The irreversible step approximation rate is calculated with or without assuming low coverage of methanol. (d) Change in Gibbs free energy (ΔG) from reference state to transition state for the possible rate-determining steps in the methanol-to-DME reaction. The reference state is the acid site and reactants in gas phase. ΔG is proportional to the rate of DME productions, and the rate-limiting step is the step with the highest ΔG.

imation because it is assumed to describe accurately the rates at the reaction conditions. This assumption is partly justified by comparing the rate of the DME formation step in the dissociative pathway calculated on the basis of both assumptions (see Figure 7a).

Both the associative and the water elimination steps are initiated by methanol adsorption. The coverage of methanol on the acid site is given by $\theta_{CH_3OH} = K_{CH_3OH}P_{CH_3OH}/(1 + K_{CH_3OH}P_{CH_3OH})$ under the assumption that no other molecules have significant coverage. The methanol coverage becomes equal to $\theta_{CH_3OH} = K_{CH_3OH}P_{CH_3OH}$ in the low coverage limit, as illustrated in Figure 7b. The low coverage approximation becomes valid at ~430 K (see Figure 7b), which means that at typical DME reaction conditions where the temperature is approximately 520 K, the low coverage approximation is valid. At P_{H_2O} = 3 bar, water condenses at 407 K,[45] as indicated by the light blue area in Figure 7c. In the following, we will therefore limit our analysis to temperatures above the condensation temperature. The rates with and without the low coverage approximation are seen in Figure 7c, which again clearly illustrates that the low coverage approximation is valid at typical DME synthesis conditions. Furthermore, the difference between the low coverage approximation and the full model is insignificant down to the condensation temperature of water.

The dissociative pathway involves two steps with the rates given by eqs 3 and 5. The actual rate of DME formation will be given by the slower of the two steps, and the rate of the DME formation step is always slower than the water elimination step (see Figure 7c). The conclusion is that the rate of the dissociative pathway is determined by the DME formation step.

On the other hand, the dissociative pathway is always faster than the associative pathway (see Figure 7c), which means that DME formation over ZSM-22 will be dominated by the dissociative pathway. It is also seen that as the temperature increases, the difference between the dissociative path and associative pathway increases.

The combination of the irreversible step approximation and low coverage approximation simplifies the rate expression considerably, and it is clearly seen from eqs 3, 5, and 7 that the rate is a simple function of pressure and the change in Gibbs free energy from the reactants in the gas phase to the transitions state. The effect of changing the pressure, at industrially relevant pressures, is much smaller than the effect of changes in the temperature when comparing pathways over a temperature range of several hundred Kelvin (see eqs 3, 5, and

dx.doi.org/10.1021/cs300722w | ACS Catal. 2013, 3, 735−745

7 and Figure 7c). The relative importance of the dissociative and associative pathway may therefore be understood on the basis of the differences in Gibbs free energies between the transition state of the dissociative and associative pathway. This presents a simple basis for understanding the relative rates as seen in Figure 7d. The two steps in the dissociative pathway have very similar slopes for ΔG, as a result of the fact that both transition states lose the same number of gas phase molecules relative to the reference state (see eqs 8 and 9). This leads to a similar entropy term in ΔG, since the loss of translational entropy dominates ΔS.

$$CH_3OH + HZ \rightarrow \text{transition state}_{\text{diss,water}} \quad (8)$$

$$2CH_3OH + HZ \rightarrow \text{transition state}_{\text{diss,DME}} + H_2O(g) \quad (9)$$

The slope of the associative pathway is steeper than the slopes of the steps in the dissociative pathway, which is a result of the transition state losing one more gas phase molecule than the steps in the dissociative pathway (see eq 10).

$$2CH_3OH + HZ \rightarrow \text{transition state}_{\text{associative}} \quad (10)$$

The above arguments based on the number of molecules lost from the reference to the transition state indicate that a crossover temperature between the dissociative and associative pathway should exist, but as seen from Figure 7d, this crossover does not take place under any industrially relevant conditions. In fact, if experiments were to be carried out at temperatures and water pressures below industrial conditions, then the dissociative pathway would still be faster than the associative pathway (see Figure 7c) to a temperature as low as ~300 K, in which case the water elimination step in the dissociative pathway would be the slowest step.

The relative importance of the associative and dissociative pathway has been studied on the basis of cluster models, which concluded that the associative pathway will dominate.[6] Cluster models find the following transition state energies relative to the gas phase reference: for the water elimination reaction, 1.45[6]/1.41[13] eV, compared with 0.88 eV in the present study; for the DME formation step, 1.27[6]/1.1[13] eV, compared with 0.83 eV in the present study; and for the associative pathway, 0.16[6]/0.13[13] eV, compared with 0.2 eV in the present study. Thus, cluster models consistently find higher activation energies for the water elimination step and lower activation energies for the associative pathway than what we calculate on ZSM-22. The comparison between the 3T and 5T cluster models and ZSM-22 indicates that the small clusters do not represent the periodic structure well, which is in line with the conclusion drawn in ref 17. It is, however, not a rigorous proof that the cluster models are not converged, which would require cluster calculations within the same implementation of DFT.[17]

DME synthesis has also been studied over tungsten polyoxymetalate Keggin clusters, where microkinetic modeling based on DFT calculations predicted that the associative path would be dominant for DME synthesis,[10] which is different from what we find over ZSM-22. The difference between the present results on ZSM-22 and the tungsten polyoxymetalates results could be speculated to originate from differences in chemical composition between tungsten polyoxymetaltes and zeolites. In addition to the different chemical compositions, another obvious difference is that Keggin tungsten polyoxometalates have oxygen with a single bond to tungsten, which does not have a parallel at internal acid sites in zeolites.

We have shown that the low coverage and irreversible step approximations are valid and that they allow us to simply compare Gibbs free energies of the transition states. We may now use this simple but accurate analysis to evaluate the effect of coadsorbed water. In the associative pathway, coadsorbed water leads to a 0.24 eV lower barrier relative to the transition state with no coadsorbed water; however, the lower activation energy due to coadsorbed water leads to a larger entropy loss relative to the gas phase. Water loses 0.0022 eV/K at a typical DME reaction temperature of 520 K, under the assumption that water loses all of its translational and rotational entropy upon adsorption. The entropy loss gives rise to an increase in Gibbs free energy of 1.12 eV at 520 K, which exceeds the 0.24 eV lowering of the activation energy induced by coadsorbed water. In fact, even at the freezing point of water, the loss in Gibbs free energy exceeds the lowering of the activation energy. We therefore suggest that a possible promotional effect of water on the associative pathway is highly unlikely and conclude that the reaction will most likely take place as seen in Figure 3.

The water elimination step in the dissociative pathway is lowered by 0.42 eV when coadsorbed water is present. The lowering of the barrier is therefore considerably less than the contribution to the free energy from the entropy lost by water adsorption (1.12 eV), and we again suggest ruling out that water has a promotional effect on the water elimination step. Water adsorption could also have an effect on the second step in the dissociative pathway, where DME is formed. Lowering of the second step will not, however, have a significant influence on the rate because the rate can be increased, at maximum, to the rate of the water elimination step, which we have just shown is unaffected by coadsorbed water. Thus, the conclusion is that water does not lead to an improved activity for the dissociative pathway and that the dissociative pathway will proceed as calculated in Figure 5.

The RPBE functional used in the present study generally gives good chemisorption energies, but it is known that van der Waals forces (vdW) are not included.[36,46] One may therefore speculate that inclusion of vdW forces could significantly change the importance of the dissociative path relative to the associative path; however, this will likely not be the case. Experimental and theoretical studies have shown that vdW forces contribute with an additional binding energy that is proportional to the number of C and O atoms.[46−50] In the following, we assume that transition states follow a similar trend and that each C or O atom contributes with 0.1 eV additional vdW binding. In the dissociative pathway, the DME formation step includes one more O atom than the water elimination step, which would decrease the difference in Gibbs free energy at 410 K between the water elimination step and DME formation step to 0.07 eV. The rate of the dissociative pathway would therefore still be determined by the DME formation step.

The associative pathway transition state would also be lowered by 0.1 eV relative to the DME formation step in the dissociative pathway. However, as seen in Figure 7d, such a small change is not sufficient to change the conclusion that the dissociative pathway dominates at relevant DME synthesis conditions. The conclusion that the dissociative path is the dominant pathway at industrially relevant conditions is therefore predicted not to change if vdW forces are included.

3.4. Acidity Activity Correlations. The activity and selectivity of a solid acid-based catalyst are often related to the acidity of the catalyst,[4,5,51] where the measures of acidity are ammonia TPD,[5] pyridine or 2,6-dimethylpyridine adsorption,[51]

dx.doi.org/10.1021/cs300722w | ACS Catal. 2013, 3, 735−745

and *n*-butylamine titration or adsorption.[4,52] In the present study, we change the intrinsic acidity, that is, the acidity per site, by using different dopants. We restrict ourselves to group III acceptors and use Al, Ga, or In as dopants. Catalytic systems with these dopants have all been experimentally realized, and it has been shown that ZSM-22 may be doped with Ga and that Ga doping changes the catalytic properties.[53,54] In-doped ZSM-22 has not been reported, but other In-doped zeolites have been reported.[32] Doping with Al, Ga, or In leads to Brønsted acid sites, and we use the ammonium ion formation energy as a measure of acidity. The average NH_4^+ formation energy over the three possible proton sites per dopant is −1.04, −0.97, and −0.89 eV for Al, Ga, and In, respectively. The acid strength, therefore, decreases as dopants come from farther down the group in the periodic table.

We find that all the investigated reactions have an inverse linear dependence on acidity (see Figure 8), where lower

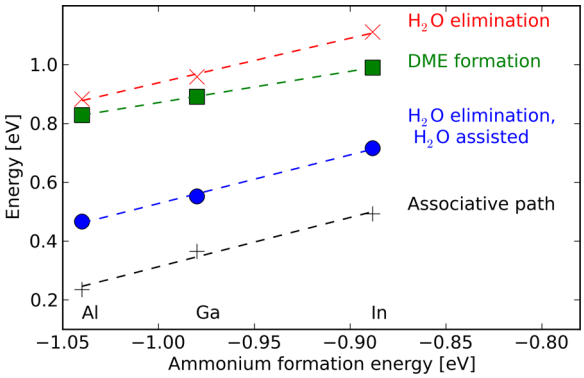

Figure 8. Transtion state energies as a function of acidity. The transition state energies are reported with reference to the gas phase molecules. H_2O elimination: $E_a = 1.56x + 2.49$, $R^2 = 0.98$. DME formation: $E_a = 1.10x + 1.97$, $R^2 = 1.00$. H_2O elimination: H_2O-assisted $E_a = 1.70x + 2.23$, $R^2 = 0.99$. Associative pathway: $E_a = 1.74x + 2.05$, $R^2 = 1.00$.

acidity leads to higher activation energies. We find that Ga doping leads to changes in transition state energies relative to Al of ∼0.1 eV, and In doping further increases the transition states ∼0.1 eV relative to Ga doping. Specifically, the H_2O elimination reactions ($E_a = 1.563x + 2.49$ and $E_a = 1.70x + 2.23$) and the associative pathway ($E_a = 1.74x + 2.05$) have similar slopes, whereas the DME formation in the dissociative pathway has a less steep slope, 1.10, compared with 1.56−1.74. The difference in slopes of the H_2O elimination and the DME formation step could lead to the H_2O elimination step becoming the rate-determining step for very weak acids. However, within the range of acid strengths studied here, the change is not large enough to overcome the difference in ΔG (see Figure 7d) between the two reactions. The similar dependence of the activation energies on acidity means that the relative importance of the dissociative and associative pathways will be only slightly influenced by changes in acidity. The dissociative pathway is therefore suggested to be predominant under DME synthesis conditions also for Ga- or In-doped ZSM-22.

The potential energy diagram for the dissociative pathway over In-, Ga-, and Al-doped ZSM-22 can be seen in Figure 9, and reaction energies and their correlation with acidity are tabulated in Table 2. We find that the adsorption energy of the intermediates also correlates with the acidity. Weaker acidity is

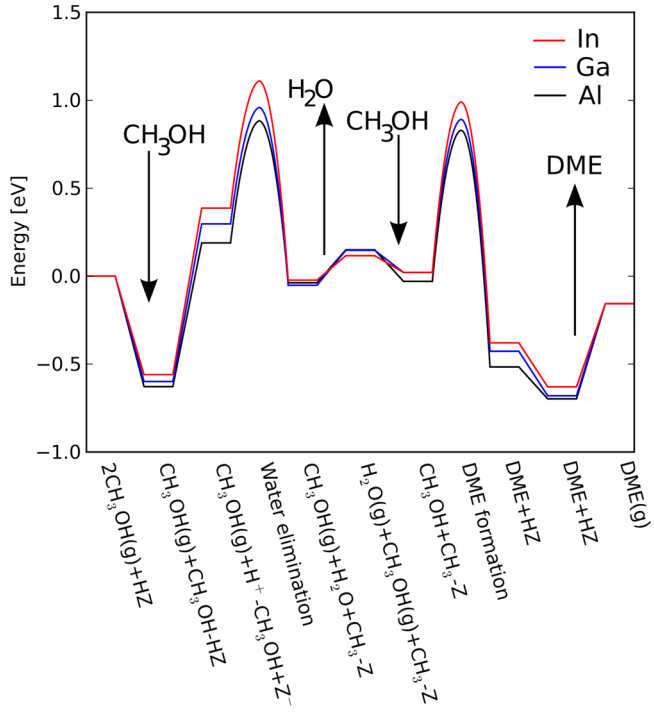

Figure 9. Electronic energies of intermediates and transition states along the dissociative pathway over In-, Ga-, or Al-doped ZSM-22.

seen to lead to weaker adsorption. The exception to this is the configurations involving an adsorbed methyl (see Table 2); here, the correlations are less clear, and the slope is very gentle. This could indicate that the correlation with the acidity is stronger when a proton is present than when the proton has been substituted with a methyl group. The general trend that adsorption and transition states scale with ammonium formation could be speculated to be linked to that charge transfer to the framework oxygen is a general feature of adsorption and transitions state configurations and, therefore, all these configurations correlate with each other. One could also speculate that transition states have steeper slopes than adsorption energies because of the larger separation in space between the acid site and the transition states than between the adsorbed molecules and the acid site. The present study shows that changing the substitutional cation leads to relatively modest changes in activation energies, and it may be speculated that this opens the possibility of fine-tuning activity and selectivity also for other acid-catalyzed reactions.

Keggin tungsten polyoxometalates have been used in a study combining DFT and kinetic measurements to understand the influence of acidity on the DME synthesis reaction[10] over this class of materials. Keggin tungsten polyoxometalates are stronger acids than zeolites,[10] and it is therefore interesting to compare with the present results on ZSM-22. The conclusion that weaker acidity leads to higher barriers is the same for tungsten polyoxometalates and ZSM-22; however, differences exist. Most importantly, the two steps in the dissociative pathway are not a linear function of acidity for tungsten polyoxometalates.[10] The least acidic tungsten polyoxometalate has significantly higher barriers than the more acidic tungsten polyoxometalates. This is attributed to a bent transition state geometry induced by the weaker acidity.[10] ZSM-22 is less acidic than tungsten polyoxometalates, but we do not find a bent transition state structure as seen in Table 1.

dx.doi.org/10.1021/cs300722w | ACS Catal. 2013, 3, 735−745

Table 2. Reaction Energies As a Function of Acidity

	Al (eV)	Ga (eV)	In (eV)	slope	intercept	R^2
acidity (NH_3(g) + HZ ↔ NH_4–Z)	−1.05	−0.99	−0.90			
2CH_3OH(g) + HZ	0.00	0.00	0.00			
CH_3OH(g) + CH_3OH + HZ	−0.63	−0.60	−0.56	0.46	−0.14	1.00
CH_3OH(g) + $CH_3OH_2^+$ + Z−	0.19	0.30	0.39	1.33	1.59	0.98
transition state water elimination	0.88	0.96	1.11	1.56	2.49	0.98
CH_3OH(g) + H_2O + CH_3–Z	−0.04	−0.05	−0.02	0.11	0.07	0.33
H_2O(g) + CH_3OH(g) + CH_3–Z	0.15	0.15	0.12	−0.23	−0.09	0.87
CH_3OH + CH_3–Z	−0.03	0.02	0.02	0.33	0.32	0.68
transition state DME formation	0.83	0.89	0.99	1.10	1.97	1.00
DME + HZ	−0.52	−0.43	−0.38	0.91	0.45	0.94
DME + HZ	−0.70	−0.68	−0.63	0.47	−0.21	0.96
DME(g) + HZ	−0.16	−0.16	−0.16			

For the tungsten polyoxometalates, the linear correlation is still not very pronounced when the least acidic data point is considered an outliner. On the basis of the data presented in ref 10, we calculate an R^2 of 0.84 and 0.79 for the water elimination and DME formation steps, respectively, which is considerably less than the 0.98 and 1.00 found in the present study. One may conclude that care should be taken when extrapolating from one class of acidic oxides to another, even though qualitative trends may be the same.

The low coverage regime is also the relevant regime for weaker acids than Al-doped ZSM-22 because a weaker adsorption strength correlates with a weaker acid strength. The rate will therefore, as is the case for Al-doped ZSM-22, depend on the free energy of the transition state relative to the gas phase. If sites can be produced that have stronger acidity than Al-doped sites, the transition to the low coverage regime will take place at higher temperatures than 430 K, and the high coverage regime could become relevant at DME reaction conditions. If such highly acidic sites exist and DME is produced with a high coverage of methanol on the acid sites, then further increasing the acidity will have little effect on the rate because both the initial and transition state are proportional to the acidity, and the apparent activation energy will therefore not vary with a further increase in acidity.

One of the major challenges in DME synthesis is to increase the temperature tolerance and limit the unwanted side reactions, such as coke formation. It could be speculated that if the unwanted side reactions have a different dependence on acidity, then an optimal acidity for DME production should exist. The present study therefore serves as the basis for further investigations into the influence of acidity on temperature tolerance and inhibition of side reactions for zeolite-based DME catalysts.

4. CONCLUSION

We have investigated the methanol-to-DME reaction over Brønsted acid sites in ZSM-22 using periodic density functional theory. DME may be produced from methanol following either the dissociative or the associative pathway, and we have investigated both pathways, including the influence of water and acidity on the potential energy landscape. We show that the dissociative pathway will be faster than the associative pathway. Water will not have any beneficial effect on the DME formation rate because the entropy loss associated with water adsorption is larger than the coadsorbed water-induced lowering of the activation energies in the dissociative and associative pathway. We have established linear correlations between acidity and activation energies and shown that weaker acids lead to higher activation energies. The changes in acidity and activation energies when Al is substituted with Ga or In is found to be relatively small, on the order of 0.1 eV, and it is proposed that using different cations may be a way to fine-tune catalysts' properties. We also find that the dissociative and associative pathways have similar dependence on acidity, which leads to the conclusion that the dissociative pathway will also dominate for weaker acids.

■ ASSOCIATED CONTENT

Supporting Information

Additional information as noted in text. This information is available free of charge via the Internet at http://pubs.acs.org/.

■ AUTHOR INFORMATION

Present Address

†Haldor Topsøe A/S Nymøllevej 55, DK-2800 Kgs. Lyngby, Denmark pogm@topsoe.dk

Notes

The authors declare the following competing financial interest(s): Poul Georg Moses is employed at Haldor Topse A/S a catalyst-producing company.

■ ACKNOWLEDGMENTS

The authors acknowledge a gift from Haldor Topsoe A/S.

■ REFERENCES

(1) Semelsberger, T. A.; Borup, R. L.; Greene, H. L. *J. Power Sources* **2006**, *156* (2), 497−511.
(2) Arcoumanis, C.; Bae, C.; Crookes, R.; Kinoshita, E. *Fuel* **2008**, *87* (7), 1014−1030.
(3) Larson, E. D.; Yang, H. *Energy Sustainable Dev.* **2004**, *8* (3), 115−126.
(4) Xu, M.; Lunsford, J. H.; Goodman, D. W.; Bhattacharyya, A. *Appl. Catal., A* **1997**, *149* (2), 289−301.
(5) Yaripour, F.; Baghaei, F.; Schmidt, I.; Perregaard, J. *Catal. Commun.* **2005**, *6* (2), 147−152.
(6) Blaszkowski, S. R.; Van Santen, R. A. *J. Phys. Chem. B* **1997**, *101* (13), 2292−2305.
(7) Schiffino, R. S.; Merrill, R. P. *J. Phys. Chem.* **1993**, *97* (24), 6425−6435.
(8) Kubelkova, L.; Novakova, J.; Nedomova, K. *J. Catal.* **1990**, *124* (2), 441−450.
(9) Spivey, J. J. *Chem. Eng. Commun.* **1991**, *110*, 123−142.
(10) Carr, R. T.; Neurock, M.; Iglesia, E. *J. Catal.* **2011**, *278* (1), 78−93.

(11) Shah, R.; Gale, J. D.; Payne, M. C. *J. Phys. Chem. B* **1997**, *101* (24), 4787−4797.
(12) Sandre, E.; Payne, M. C.; Gale, J. D. *Chem. Commun.* **1998**, *22*, 2445−2446.
(13) Lesthaeghe, D.; Van Speybroeck, V.; Marin, G. B.; Waroquier, M. *Angew. Chem., Int. Ed.* **2006**, *45* (11), 1714−1719.
(14) Sinclair, P. E.; Catlow, C. R. A. *J. Chem. Soc., Faraday Trans.* **1997**, *93* (2), 333−345.
(15) Svelle, S.; Visur, M.; Olsbye, U.; Saepurahman; Bjørgen, M. *Top. Catal.* **2011**, *54* (13−15), 897−906.
(16) Jiang, Y.; Hunger, M.; Wang, W. *J. Am. Chem. Soc.* **2006**, *128* (35), 11679−11692.
(17) Tuma, C.; Sauer, J. *Phys. Chem. Chem. Phys.* **2006**, *8* (34), 3955−3965.
(18) Hytha, M.; Stich, I.; Gale, J. D.; Terakura, K.; Payne, M. C. *Chem.—Eur. J.* **2001**, *7* (12), 2521−2527.
(19) Shah, R.; Gale, J. D.; Payne, M. C. *J. Phys. Chem.* **1996**, *100* (28), 11688−11697.
(20) Shah, R.; Payne, M. C.; Lee, M. H.; Gale, J. D. *Science* **1996**, *271* (5254), 1395−1397.
(21) Stich, I.; Gale, J. D.; Terakura, K.; Payne, M. C. *J. Am. Chem. Soc.* **1999**, *121* (14), 3292−3302.
(22) Vos, A. M.; Rozanska, X.; Schoonheydt, R. A.; Van Santen, R. A.; Hutschka, F.; Hafner, J. *J. Am. Chem. Soc.* **2001**, *123* (12), 2799−2809.
(23) Teketel, S.; Olsbye, U.; Lillerud, K. P.; Beato, P.; Svelle, S. *Microporous Mesoporous Mater.* **2010**, *136* (1−3), 33−41.
(24) Li, J.; Wei, Y.; Liu, G.; Qi, Y.; Tian, P.; Li, B.; He, Y.; Liu, Z. *Catal. Today* **2011**, *171* (1), 221−228.
(25) Verboekend, D.; Thomas, K.; Milina, M.; Mitchell, S.; Perez-Ramirez, J.; Gilson, J. P. *Catal. Sci. Technol.* **2011**, *1* (8), 1331−1335.
(26) Teketel, S.; Svelle, S.; Lillerud, K. P.; Olsbye, U. *ChemCatChem* **2009**, *1* (1), 78−81.
(27) Cui, Z. M.; Liu, Q.; Song, W. G.; Wan, L. J. *Angew. Chem., Int. Ed.* **2006**, *45* (39), 6512−6515.
(28) Cui, Z. M.; Liu, Q.; Ma, Z.; Bian, S. W.; Song, W. G. *J. Catal.* **2008**, *258* (1), 83−86.
(29) Cui, Z. M.; Liu, Q.; Bain, S. W.; Zhuo, M.; Song, W. G. *J. Phys. Chem. C* **2008**, *112* (7), 2685−2688.
(30) Raybaud, P.; Patrigeon, A.; Toulhoat, H. *J. Catal.* **2001**, *197* (1), 98−112.
(31) Blaszkowski, S. R.; Van Santen, R. A. *J. Am. Chem. Soc.* **1997**, *119* (21), 5020−5027.
(32) Berndt, H.; Martin, A.; Kosslick, H.; Lucke, B. *Microporous Mater.* **1994**, *2* (3), 197−204.
(33) Bahn, S. R.; Jacobsen, K. W. *Comput. Sci. Eng.* **2002**, *4* (3), 56−66.
(34) Enkovaara, J.; Rostgaard, C.; Mortensen, J. J.; Chen, J.; Dulak, M.; Ferrighi, L.; Gavnholt, J.; Glinsvad, C.; Haikola, V.; Hansen, H. A.; Kristoffersen, H. H.; Kuisma, M.; Larsen, A. H.; Lehtovaara, L.; Ljungberg, M.; Lopez-Acevedo, O.; Moses, P. G.; Ojanen, J.; Olsen, T.; Petzold, V.; Romero, N. A.; Stausholm-Møller, J.; Strange, M.; Tritsaris, G. A.; Vanin, M.; Walter, M.; Hammer, B.; Hakkinen, H.; Madsen, G. K. H.; Nieminen, R. M.; Nørskov, J. K.; Puska, M.; Rantala, T. T.; Schiøtz, J.; Thygesen, K. S.; Jacobsen, K. W. *J. Phys.: Condens. Matter* **2010**, *22*, 25.
(35) Mortensen, J. J.; Hansen, L. B.; Jacobsen, K. W. *Phys. Rev. B: Condens. Matter Mater. Phys.* **2005**, *71* (3), 1−11.
(36) Hammer, B.; Hansen, L. B.; Nørskov, J. K. *Phys. Rev. B: Condens. Matter Mater. Phys.* **1999**, *59* (11), 7413−7421.
(37) Marler, B. *Zeolites* **1987**, *7* (5), 393−397.
(38) Henkelman, G.; Uberuaga, B. P.; Jonsson, H. *J. Chem. Phys.* **2000**, *113* (22), 9901−9904.
(39) Yaws, C. L. *The Yaws Handbook of Thermodynamic Properties for Hydrocarbons and Chemicals*; Knovel: New York, 2009.
(40) *Handbook of Chemistry and Physics*, 90th ed.; CRC Press: Boca Raton, 2009.
(41) Nørskov, J. K.; Abild-Pedersen, F.; Studt, F.; Bligaard, T. *Proc. Natl. Acad. Sci. U. S. A.* **2011**, *108* (3), 937−943.
(42) Bucko, T.; Benco, L.; Hafner, J.; Angyan, J. G. *J. Catal.* **2011**, *279* (1), 220−228.
(43) Goltl, F.; Hafner, J. *Microporous Mesoporous Mater.* **2013**, *166* (0), 176−184.
(44) Hellman, A.; Baerends, E. J.; Biczysko, M.; Bligaard, T.; Christensen, C. H.; Clary, D. C.; Dahl, S.; van Harrevelt, R.; Honkala, K.; Jonsson, H.; Kroes, G. J.; Luppi, M.; Manthe, U.; Nørskov, J. K.; Olsen, R. A.; Rossmeisl, J.; Skúlason, E.; Tautermann, C. S.; Varandas, A. J. C.; Vincent, J. K. *J. Phys. Chem. B* **2006**, *110* (36), 17719−17735.
(45) Smith, J. M.; Van Ness, H. C.; Abbott, M. M. *Introduction to Chemical Engineering Thermodynamics*; International ed.; McGraw-Hill: New York, 2001.
(46) Moses, P. G.; Mortensen, J. J.; Lundqvist, B. I.; Nørskov, J. K. *J. Chem. Phys.* **2009**, *130*, 104709.
(47) Eder, F.; Stockenhuber, M.; Lercher, J. A. *J. Phys. Chem. B* **1997**, *101* (27), 5414−5419.
(48) Mukti, R. R.; Jentys, A.; Lercher, J. A. *J. Phys. Chem. C* **2007**, *111* (10), 3973−3980.
(49) Goltl, F.; Hafner, J. *J. Chem. Phys.* **2011**, *134*, 6.
(50) Goltl, F.; Gruneis, A.; Bucko, T.; Hafner, J. *J. Chem. Phys.* **2012**, *137* (11), 114111.
(51) Campelo, J. M.; Garcia, A.; Herencia, J. F.; Luna, D.; Marinas, J. M.; Romero, A. A. *J. Catal.* **1995**, *151* (2), 307−314.
(52) Wang, I.; Chang, W. F.; Shiau, R. J.; Wu, J. C.; Chung, C. S. *J. Catal.* **1983**, *83* (2), 428−436.
(53) Singh, A. P.; Reddy, K. R. *Zeolites* **1994**, *14* (4), 290−294.
(54) Asensi, M. A.; Corma, A.; Martinez, A.; Derewinski, M.; Krysciak, J.; Tamhankar, S. S. *Appl. Catal., A* **1998**, *174* (12), 163−175.